Comparative Analysis of Physical and Gas-Sensing Properties of Cobalt-Doped Zirconium Dioxide Thin Films

Hanaa Kadem Essa[1], Rushdi Ibrahim Jasim[1], Wafaa Hameed Abbas[2], Muhaned Zaidi[3], Saja Faez Hassan[1] and Reem Sami Ali[4]

[1]*Department of Physics, College of Education, Mustansiriyah University, 10052 Baghdad, Iraq*
[2]*Department of Studies and Planning, Ministry of Higher Education and Scientific Research, 10001 Baghdad, Iraq*
[3]*Department of Medical Physics, College of Science, Al-Manara University, 62001 Amarah, Iraq*
[4]*Department of Physics, College of Education, Mustansiriyah University, 10052 Baghdad, Iraq*
reemphy81@uomustansiriyah.edu.iq

Keywords: ZrO_2:Co Thin Films, CSP, XRD, AFM, Optical Properties, Gas Sensing.

Abstract: Cobalt-doped zirconium dioxide (ZrO_2:Co) nanostructured thin films were successfully deposited on glass substrates using the chemical spray pyrolysis (CSP) technique. X-ray diffraction revealed a polycrystalline orthorhombic structure with a predominant (111) orientation. Cobalt incorporation initially enhanced crystallinity at 1% doping, as evidenced by increased peak intensity and grain growth from 11.82 nm to 19.04 nm. However, further doping to 3% Co induced lattice disorder, slightly reducing crystalline quality. Atomic force microscopy demonstrated that Co doping significantly refined the surface morphology, reducing both the average particle size (from 68.57 nm to 36.04 nm) and surface roughness, indicating the formation of smoother, more compact films. Optical transmittance measurements showed high transparency (92.4-96.5%) in the visible region, which decreased with increasing Co content. The optical band gap narrowed systematically from 5.25 eV to 5.15 eV with Co doping, ascribed to the existence of defect states and impurity levels within the ZrO_2 band structure. Gas-sensing tests at 225 ppm NO_2 and 125 °C revealed that Co doping substantially enhanced the sensor response, with the 3% Co-doped film exhibiting the greatest resistance modulation. However, sensitivity calculations demonstrated a decrease in sensor response with increasing Co concentration.

1 INTRODUCTION

One of the most significant and popular types of solid catalysts is metal oxides, which can be utilized as both supports and active phases [1], [2]. Metal oxides constitute the largest class of catalysts in heterogeneous catalysis and are used for their acid-base and redox properties [3]-[6]. (ZrO_2) has been employed as a support for dispersing noble and transition metals for specific catalytic applications due to its exceptional catalytic capabilities across a variety of processes [7], [8]. ZrO_2 is a well-known solid-acid catalyst and exhibits n-type semiconductor behaviour [9]-[13]. Cobalt (Co) is one of the most effective transition metal dopants that can modify the structural, optical, and electrical behavior of metal oxide semiconductors [14]-[16]. The presence of cobalt ions in the ZrO_2 lattice can significantly modify the defect structure, grain size, and electronic properties of the material [17], [18]. The substitution of Zr^{4+} ions by Co ions, with the resulting localized energy levels and oxygen vacancies [19], [20], enhances charge-carrier transport and surface reactivity [21]. The goal of this study is to look into the impact of cobalt doping on the physical and sensing properties of ZrO_2 nanostructured thin films. Cobalt-doped ZrO_2 thin films were prepared using CSP, a simple, cost-effective, and versatile method. The prepared films were subsequently characterized to evaluate their structural, optical, and sensing properties and to understand the role of cobalt incorporation in improving the functional performance of ZrO_2 thin films.

2 EXPERIMENTAL

CSP was used for forming ZrO_2 thin films. The precursor was $ZrCl_2$ (99.99% purity) from Sigma-Aldrich. Cobalt chloride dopant (99.98% purity, Merck, Germany) was added to the precursor solution at volumetric ratios of 1% and 3%. Filtered air was sprayed onto glass substrates at 10^5 Pa. To avoid excessive cooling, the flow rate was set to 5 ml/min, and the deposition period was 10 seconds, with a 2-minute break. There was a 28 cm distance between the spout and the substrate, and the base body temperature during deposition was maintained at 450°C. The film thickness obtained by the gravimetric approach is 330 ± 20 nm. AFM was used to study surface topography, and XRD was used to characterize the film structure. A UV-visible Shimadzu double-beam spectrophotometer was used to record the transmittance spectra of the as-deposited thin films in the 300-900 nm wavelength range. Gas sensitivity was evaluated as the percentage change in the film resistance upon exposure to the target gas. The measurements were carried out in a custom-designed cylindrical chamber with a radius of 8 cm and a height of 16 cm.

3 RESULTS AND DISCUSSION

Figure 1 shows the X-ray diffraction (XRD) patterns of Co-doped ZrO2 thin films with cobalt concentrations of 0%, 1%, and 3%. The diffraction patterns confirm the formation of an orthorhombic crystalline structure with a preferred orientation along the (111) plane. Additional diffraction peaks corresponding to the (200), (220), and (222) crystallographic planes were also observed. The diffraction peaks of the undoped ZrO2 film are consistent with JCPDS card No. 37-1484, confirming the successful formation of the crystalline ZrO2 phase.

With increasing cobalt concentration, slight shifts in the diffraction peak positions and changes in peak intensity were observed, indicating the incorporation of Co ions into the ZrO2 crystal lattice. The increase in peak intensity at low cobalt concentration suggests improved crystallinity and better crystallite orientation. However, further increasing the cobalt concentration resulted in a reduction of peak intensity, indicating a slight deterioration in crystalline quality. This behavior may be attributed to lattice distortion and internal stress caused by excessive cobalt incorporation, which hinders crystallite growth and introduces structural disorder [14], [18], [22].

The crystallite size was estimated using the Scherrer method [23], [24], and the calculated values are summarized in Table 1. The crystallite size increased from 11.82 nm for the undoped film to 19.04 nm and 21.10 nm for the films containing 1% and 3% cobalt, respectively. The increase in crystallite size indicates enhanced crystal growth, which is likely associated with the incorporation of cobalt ions into the ZrO2 lattice and the reduction of grain boundary defects.

The dislocation density and lattice strain were calculated from the XRD data [26]–[28]. As presented in Figure 2 and Table 1, both parameters decreased with increasing cobalt concentration, indicating improved crystalline quality and reduced lattice imperfections. The reduction in dislocation density and lattice strain suggests that cobalt doping promotes better structural ordering and decreases the number of crystal defects within the films. Similar behavior has been reported by Shi et al. [29]. The calculated values of crystallite size, full width at half maximum (FWHM), lattice strain, and dislocation density for the undoped and Co-doped ZrO2 thin films are summarized in Table 1.

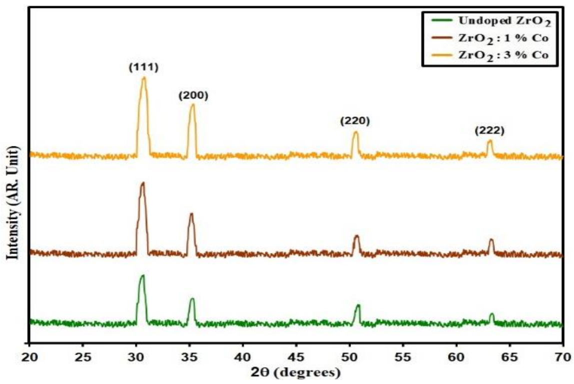

Figure 1: XRD patterns of undoped and Co-doped ZrO_2 thin films.

The surface topography of ZrO_2 thin films doped with 0%, 1%, and 3% cobalt was examined using AFM (Table 2). Figure 3 presents representative AFM images, revealing a uniform grain distribution composed of columnar aggregates, with no noticeable holes or fissures. The average particle sizes decrease with increasing Co content, measuring 68.57 nm, 43.20 nm, and 36.04 nm for 0%, 1%, and 3% Co, respectively. Correspondingly, average roughness (Ra) and root mean square roughness (RMS), decrease from 9.25 nm to 3.78 nm and from 3.37 nm to 2.65 nm, respectively, indicating a smoother surface with higher doping levels. The observed variations in particle size and roughness (Pav and RMS) between undoped and Co-doped films suggest that cobalt incorporation influences nucleation and growth processes. Additionally, factors such as surface diffusion temperature, deposition kinetics, and dopant concentration play a significant role in controlling the surface morphology and overall film roughness [30], [31].

The optical transmittance spectra of the deposited films are presented in Figure 4. All films exhibit high optical transmittance in the visible region, with values ranging from 92.4% to 96.5%. The transmittance gradually increases with increasing wavelength, indicating reduced optical absorption in the near-infrared region. This behavior suggests that photons with lower energy are insufficient to promote electrons across the optical band gap, resulting in lower absorption and higher transmittance [32], [33].

Figure 5 shows the absorbance spectra of the undoped and Co-doped ZrO2 thin films. The undoped film exhibits the lowest absorbance, whereas the absorbance increases progressively with increasing cobalt concentration. This behavior is attributed to the incorporation of cobalt ions into the ZrO2 lattice, which introduces additional defect states and localized energy levels within the band structure. These states facilitate electronic transitions and increase the probability of photon absorption, thereby enhancing the light-harvesting capability of the doped films [36], [37].

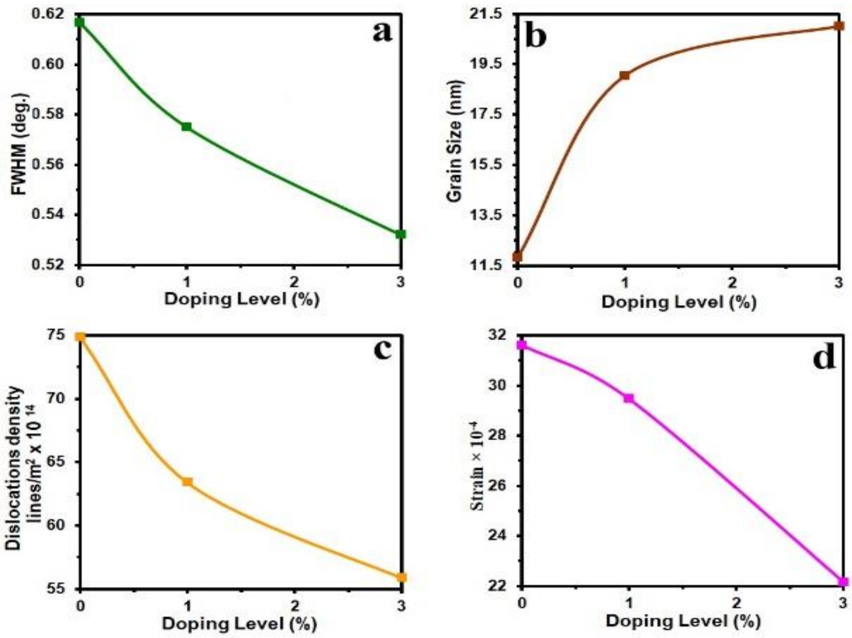

Figure 2: Variation of structural parameters (FWHM, crystallite size, dislocation density, and lattice strain) with Co doping concentration.

Table 1: Variation of structural parameters (FWHM, crystallite size, dislocation density, and lattice strain) with Co doping concentration.

Specimen	2 θ (°)	(hkl) Plane	FWHM (°)	E_g (eV)	D (nm)	δ (× 10^{14}) (lines/m²)	ε(× 10^{-4})
Undoped ZrO_2	111	30.59	0.62	5.25	11.82	74.84	31.62
ZrO_2: 1% Co	111	30.54	0.59	5.20	19.04	63.41	29.47
ZrO_2: 3% Co	111	30.50	0.53	5.15	21.01	55.87	22.16

Table 2: AFM surface parameters of undoped and Co-doped ZrO_2 thin films.

Samples	Average Particle size (nm)	R_a (nm)	RMS (nm)
Undoped ZrO_2	68.57	9.25	7.37
ZrO_2: 1% Co	43.20	8.41	5.45
ZrO_2: 3% Co	36.04	3.78	2.65

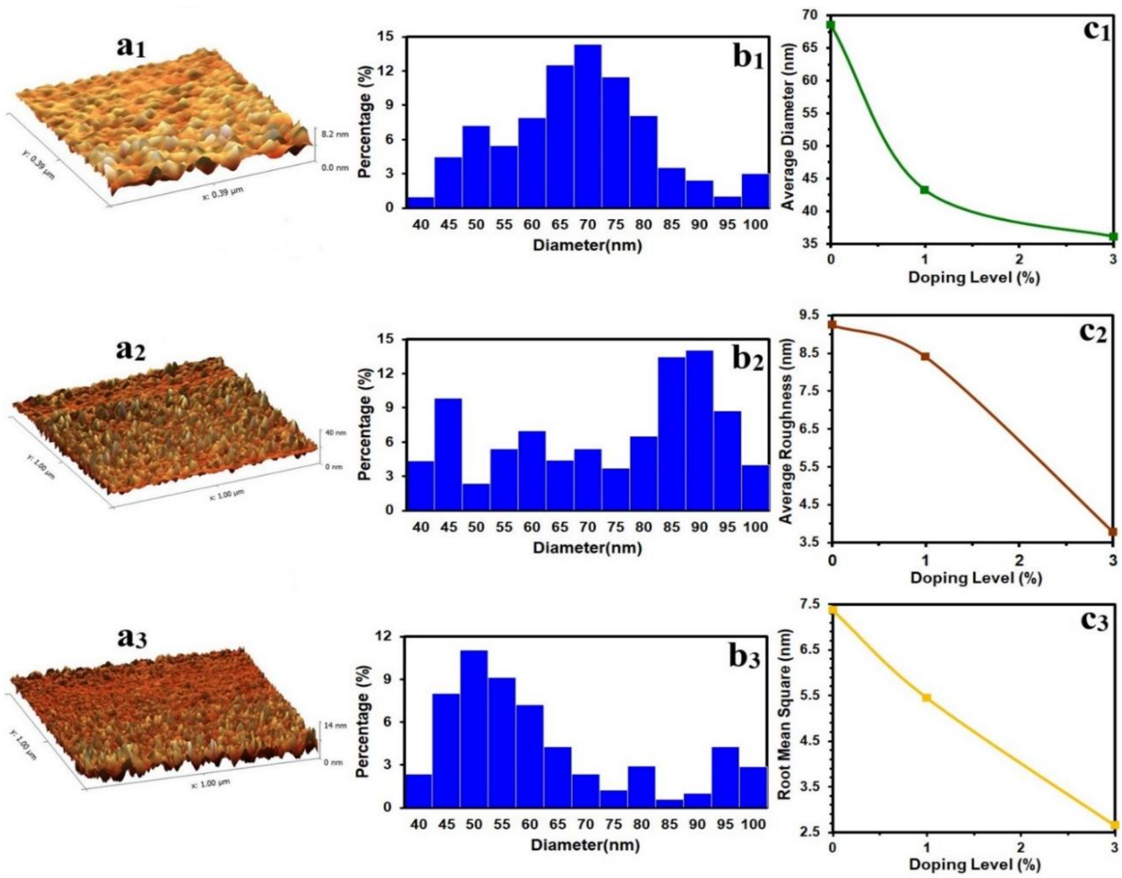

Figure 3: AFM surface morphology of undoped and Cu-doped Co_3O_4 thin films.

The absorption coefficient was determined from the optical absorbance and film thickness [38]. The calculated values indicate that cobalt doping enhances the optical absorption of the films, which is consistent with the observed increase in absorbance. The improvement in optical absorption can be attributed to the formation of defect-related energy states and the modification of the electronic structure caused by cobalt incorporation.

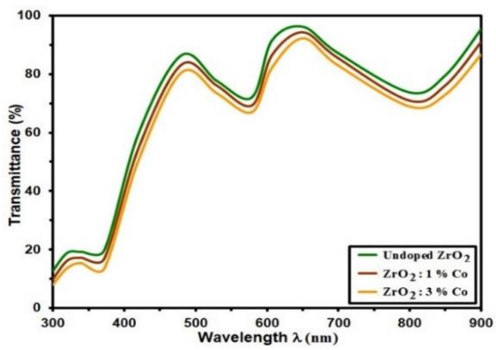

Figure 4: Optical transmittance spectra of undoped and Cu-doped Co_3O_4 thin films.

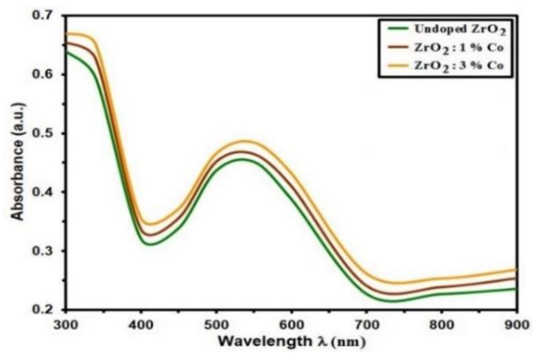

Figure 5: Optical absorbance spectra of undoped and Cu-doped Co_3O_4 thin films.

Figure 6 presents the absorption coefficient spectra of the undoped and Co-doped ZrO2 thin films. The absorption coefficient increases with increasing cobalt concentration, indicating enhanced optical absorption after doping. A sharp increase in the absorption coefficient is observed near the absorption edge, followed by a gradual decrease at higher wavelengths. The absorption coefficient reaches values of approximately 10^4 cm^{-1} or higher, confirming the presence of strong direct electronic transitions in the films. The enhanced absorption observed in the Co-doped samples is attributed to modifications of the electronic structure and the formation of defect-related energy states that facilitate photon absorption [39], [40].

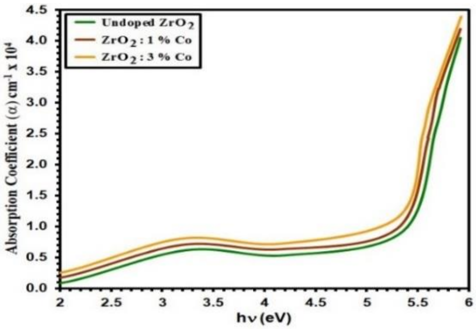

Figure 6: Absorption coefficient (α) as a function of photon energy (hν) for undoped and Cu-doped Co_3O_4 thin films.

The direct optical band gap was estimated using the Tauc method [41]. As shown in Figure 7, the optical band gap decreases with increasing cobalt concentration. The band gap is reduced from 5.25 eV for the undoped film to approximately 5.15 eV for the film containing the highest cobalt concentration. This reduction is attributed to the introduction of cobalt-related defect states within the forbidden energy gap, which create intermediate energy levels and facilitate electronic transitions at lower photon energies. In addition, cobalt incorporation increases structural disorder, contributing to the observed band-gap narrowing [42], [43].

The extinction coefficient was calculated from the optical absorption data [44]. Figure 8 shows that the extinction coefficient exhibits relatively high values in the ultraviolet region and gradually decreases with increasing wavelength. This behavior reflects the strong absorption of high-energy photons by the films. The persistence of nonzero extinction coefficient values below the fundamental absorption edge indicates the existence of defect- and impurity-related electronic states introduced by structural imperfections and cobalt incorporation [45].

The refractive index was determined from the measured optical parameters [46]. As illustrated in Figure 9, the refractive index increases with wavelength for all samples, exhibiting normal dispersion behavior. However, the refractive index decreases with increasing cobalt concentration. This reduction is attributed to changes in the electronic polarizability and structural modification of the ZrO2 lattice caused by cobalt incorporation. These changes alter the interaction between light and the material, resulting in a lower refractive index for the doped thin films [47], [48].

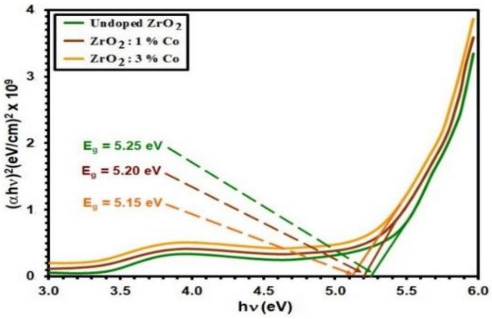

Figure 7: Tauc plots ($(\alpha h\nu)^2$ versus hν) of undoped and Cu-doped Co_3O_4 thin films.

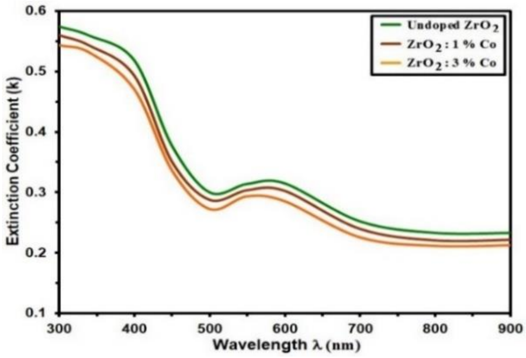

Figure 8: Extinction coefficient spectra of undoped and Cu-doped Co_3O_4 thin films.

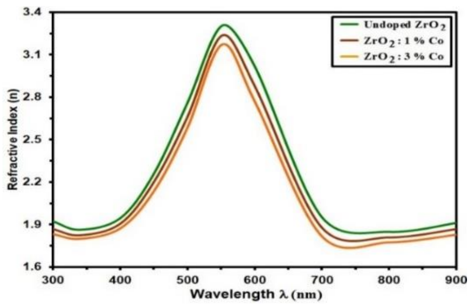

Figure 9: Refractive index spectra of undoped and Cu-doped Co_3O_4 thin films.

Figure 10 presents the dynamic resistance response of the undoped and Co-doped ZrO2 thin films upon exposure to 225 ppm NO2 at an operating temperature of 125 °C. The observed resistance changes are attributed to the interaction between NO2 molecules and the adsorbed oxygen species on the film surface, which modifies the charge carrier concentration and affects electrical conductivity. In addition, this interaction alters the potential barrier at the grain boundaries, influencing charge transport through the sensing layer. Among the investigated samples, the film doped with 3 wt.% cobalt exhibited the highest resistance, indicating that cobalt incorporation significantly affects the sensing behavior of the films and enhances their response toward NO2 gas [49]–[51].

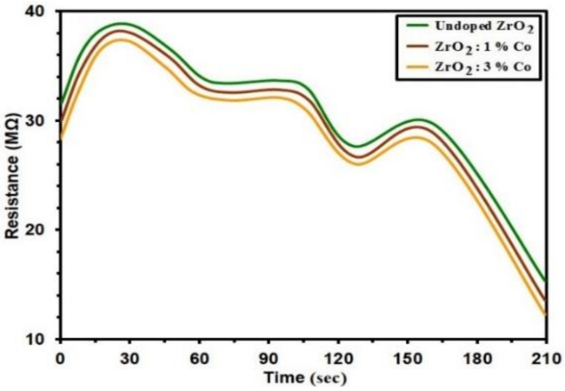

Figure 10: Resistance response of undoped and Cu-doped Co_3O_4 thin films under NO_2 gas exposure.

The gas sensor sensitivity was calculated from the measured resistance values [52]. Figure 11 compares the sensitivity of the undoped and Co-doped ZrO2 thin films toward NO2 gas. The results indicate that sensor sensitivity decreases with increasing cobalt concentration. This behavior is attributed to enhanced charge carrier recombination and changes in the electrical properties of the sensing layer caused by cobalt incorporation. The reduction in the number of free charge carriers increases the electrical resistance of the films and consequently lowers their sensitivity to NO2 gas exposure [53].

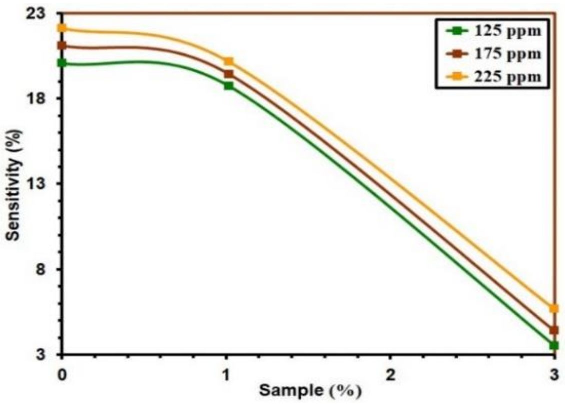

Figure 11: NO_2 gas sensitivity of undoped and Cu-doped Co_3O_4 thin films.

4 CONCLUSIONS

Undoped and Co-doped ZrO_2 thin films were successfully synthesized using the chemical spray pyrolysis (CSP) technique, yielding uniform and adherent coatings. Structural analysis confirmed the formation of polycrystalline orthorhombic films with a predominant (111) orientation. The incorporation of cobalt enhanced crystallite growth and improved overall crystalline quality, as indicated by increased grain size along with reduced microstrain and dislocation density. Morphological studies revealed that Co doping significantly refined the surface features, producing smoother and more compact films with decreased particle size and surface roughness. Optical characterization showed that all films maintained high transparency in the visible region, while the optical band gap decreased progressively with increasing Co concentration. This band gap narrowing is attributed to the formation of localized defect states and impurity energy levels within the band structure. Gas-sensing measurements toward NO_2 indicated that Co doping increased the baseline resistance of the films; however, the sensitivity declined at higher doping levels.

ACKNOWLEDGMENTS

This research is supported by Mustansiriyah University.

REFERENCES

[1] L. Nikoshvili, O. Manaenkov, O. Kislitsa, M. Sulman, V. Matveeva, and L. Kiwi-Minsker, “Functionalized porous organic polymers as supports for metal-containing heterogeneous catalysts: the role of polymer functionalities,” Catalysis Reviews, pp. 1-46, 2026, [Online]. Available: https://doi.org/10.1080/catalrev.2026.000000.

[2] M. Arivazhagan, S. Paramasivam, L. Gnanasekaran, S. Prabu, S. Boonyuen, A. Ravikumar, and J. Jakmunee, “Current status and future challenges of transition-metal oxides as enzyme-mimetics for detection of clinically relevant biomarkers: a comprehensive review,” Microchimica Acta, vol. 193, no. 2, p. 118, 2026, [Online]. Available: https://doi.org/10.1007/s00604-026-00000-0.

[3] J. C. Védrine, “Importance, features and uses of metal oxide catalysts in heterogeneous catalysis,” Chinese Journal of Catalysis, vol. 40, no. 11, pp. 1627-1636, 2019, [Online]. Available: https://doi.org/10.1016/S1872-2067(19)63456-0.

[4] G. Allada, P. K. Matsa, K. Gogoi, and S. Chakraborty, “Regulating Electronic Functionality in Lindqvist Polyoxometalates: A Molecular Approach to Tunable Metal Oxides,” Chemistry of Materials, 2026, [Online]. Available: https://doi.org/10.1021/acs.chemmater.6b00000.

[5] D. Chen, Y. Chai, J. Lin, and X. Wang, “Atomically tailored non-noble metal-based catalysts toward efficient propane dehydrogenation,” Chemical Communications, 2026, [Online]. Available: https://doi.org/10.1039/D6CC00000A.

[6] S. A. Karakoulia, A. A. Marianou, C. M. Michailof, and A. A. Lappas, “Preparation, Characterization, and Catalytic Performance of Metal-Based Heterogeneous Catalysts for Glucose Oxidation to Gluconic Acid,” Catalysts, vol. 16, no. 2, p. 135, 2026, [Online]. Available: https://doi.org/10.3390/catal16020135.

[7] Z. Y. Hussien, A. Q. Moften, and M. A. Abdulrehman, “Review of zirconia (ZrO2) biomedical applications: Advanced manufacturing techniques and materials properties,” Revue des Composites et des Materiaux Avances, vol. 35, no. 2, p. 345, 2025, [Online]. Available: https://doi.org/10.18280/rcma.350205.

[8] Y. Huang and Z. Duan, “Research progress in Cu-ZrO2 catalysts: a systematic review of their preparation, doping, and applications,” Journal of Materials Chemistry A, vol. 13, no. 6, pp. 4043-4089, 2025, [Online]. Available: https://doi.org/10.1039/D5TA00000A.

[9] P. Kumar, A. K. Rahul, P. Kaur, and J. Kaur, “Structure, Properties and Application of Metal Oxide,” in Metal Oxides, CRC Press, pp. 3-21, 2025.

[10] N. A. H. Sazalli, C. C. Kee, S. H. Osman, B. T. Goh, R. Ahmad, P. K. Jiwanti, and Y. H. Wong, “Advances in ZrO2 gate dielectrics: materials, optimization strategies, and electronic applications,” Journal of Materials Science: Materials in Electronics, vol. 36, no. 20, p. 1214, 2025, [Online]. Available: https://doi.org/10.1007/s10854-025-00000-0.

[11] S. Dwivedi, “Methods for Synthesis of Metal Oxide-based High-K Dielectrics,” in Metal Oxide-based High-K Dielectrics, CRC Press, pp. 56-80, 2025.

[12] K. Kim, “Fabrication and characterization of ferroelectric HfxZr1-xOy layers for novel nanosheet devices: from high-k to ferroelectric behaviors,” Ph.D. dissertation, Technische Universität Wien, 2023.

[13] Z. Zheng, “Oxide Semiconductor-Based Ferroelectric/Antiferroelectric Field-Effect Transistors for Beol-Compatible Memory and Memory-Centric Computing,” Ph.D. dissertation, National University of Singapore, 2024.

[14] G. Murtaza, Y. Abbas, and F. Ahmed, “Theoretical and experimental study of structural, electronic and optical properties of cobalt-doped zinc oxide,” Physica B: Condensed Matter, vol. 712, 417283, 2025, [Online]. Available: https://doi.org/10.1016/j.physb.2025.417283.

[15] R. Rahaman, M. Sharmin, and J. Podder, “The effect of cobalt doping on the structure and properties of copper oxide thin films: evolution in surface morphology, p-to n-type carrier transition and enhancement optoelectronic behavior,” International Journal of Modern Physics B, vol. 39, no. 17, 2550145, 2025, [Online]. Available: https://doi.org/10.1142/S021797922550145X.

[16] J. Mangaiyarkkarasi, D. Sivaganesh, and S. Sasikumar, “Impact of cobalt doping on the structural, optical, and electronic characteristics of xCo: NiO crystal lattice,” Transition Metal Chemistry, vol. 50, no. 5, pp. 673-685, 2025, [Online]. Available: https://doi.org/10.1007/s11243-025-00000-0.

[17] R. G. Balkanloo and A. Esmaeili, “The functional role of ZrO2 nanoparticles in comparing advanced applications of WO3-Fe2O3-ZrO2 and WO3-Fe2O3 nanocomposites synthesized by the solid-state reaction method: a comparative study of impedance spectroscopy, dielectric behavior, and magnetic properties,” Materials Science and Engineering: B, vol. 327, 119296, 2026, [Online]. Available: https://doi.org/10.1016/j.mseb.2026.119296.

[18] P. Gayathri, V. Balasubramani, D. S. Priya, T. Ali, Z. Ahmad, and M. Shkir, “Investigation of photo-induced charge carrier transport phenomena in Cu/ZrO2@Cd/n-Si MIS Schottky barrier diodes for high-performance optoelectronic applications,” Journal of Materials Science: Materials in Electronics, vol. 36, no. 32, p. 2077, 2025, [Online]. Available: https://doi.org/10.1007/s10854-025-00000-1.

[19] A. M. Hassan, H. A. Alyousef, A. S. Ali, S. A. Issa, and H. M. Zakaly, “Cobalt-doped zirconium dioxide nanoparticles: enhancement of structural and optical properties, as well as radiative efficiency, for photocatalysis and radiation shielding applications,” Journal of Materials Science: Materials in Electronics, vol. 36, no. 14, p. 813, 2025, [Online]. Available: https://doi.org/10.1007/s10854-025-00000-2.

[20] N. Madhu, K. P. Biju, and A. A. Gafoor, “Oxygen Vacancy Mediated Enhanced Luminescence and Photocatalysis in Coprecipitated ZrO2 Nano Particles,” Journal of Fluorescence, vol. 35, no. 10, pp. 10153-10166, 2025, [Online]. Available: https://doi.org/10.1007/s10895-025-00000-0.

[21] S. Sun, Y. Zhang, J. Wu, F. Zhang, R. Yan, and C. Wen, “Interfacial Engineering of ZrO2@Co-MOF Heterostructures for Highly Selective Electrocatalytic Glycerol Oxidation to Formic Acid,” New Journal of Chemistry, 2026, [Online]. Available: https://doi.org/10.1039/D6NJ00000A.

[22] W. Ahmed and J. Iqbal, “Co doped ZrO2 nanoparticles: an efficient visible light triggered photocatalyst with enhanced structural, optical and dielectric characteristics,” Ceramics International, vol. 46, no. 16, pp. 25833-25844, 2020, [Online]. Available: https://doi.org/10.1016/j.ceramint.2020.03.000.

[23] H. S. Al-Rikabi, M. H. Al-Timimi, and W. H. Albanda, “Morphological and optical properties of MgO1-xZnSx thin films,” Digest Journal of Nanomaterials and Biostructures, vol. 17, no. 3, pp. 889-897, 2022.

[24] S. Mahmood Hussein, T. H. Mubarak, S. M. Ali Ridha, and J. Al-Zanganawee, “Synthesis and characterizations of nano magnetic particles (Co-Ni Fe2O4) ferrite by co-precipitation and biomedical application,” International Journal of Nanoelectronics and Materials, vol. 16, no. 1, pp. 135-144, 2023.

[25] R. R. Ahmed, T. H. Mubarak, and I. H. Mohamed, “A study of structural and chemical properties of Ni1-xZnxFe2O4 ferrite powder prepared by co-precipitation method,” Digest Journal of Nanomaterials and Biostructures, vol. 17, no. 3, pp. 741-748, 2022.

[26] M. B. Jumaa, T. H. Mubarak, and A. M. Mohammad, "Synthesis and characterization of spinel ferrite Co0.8Fe2.2O4 nanoparticle," Journal of University of Anbar for Pure Science, vol. 15, no. 2, pp. 74-82, 2021.

[27] R. Kuekha, T. H. Mubarak, and B. Azhdar, "Synthesis, structural, magnetic, and dielectric properties of Ni2+, Mn2+ Co-substituted CoFe2O4 nanoferrites using sol-gel auto combustion method," Materials Science and Engineering: B, vol. 292, 116411, 2023, [Online]. Available: https://doi.org/10.1016/j.mseb.2023.116411.

[28] F. S. Ahmed, N. Y. Ahmed, R. S. Ali, N. F. Habubi, K. H. Abass, and S. S. Chiad, "Effects of substrate type on some optical and dispersion properties of sprayed CdO thin films," NeuroQuantology, vol. 18, no. 3, pp. 56-65, 2020.

[29] T. Shi, Z. Tang, P. Liang, X. Zhang, D. Zhang, Q. Shao, and H. Chen, "ZrO2@Ag@SiO2 sandwich structure with high SERS enhancement effect and stability," The Journal of Physical Chemistry C, vol. 124, no. 47, pp. 25967-25974, 2020, [Online]. Available: https://doi.org/10.1021/acs.jpcc.0c00000.

[30] A. Hazim, H. M. Abduljalil, and A. Hashim, "Analysis of structural and electronic properties of novel (PMMA/Al2O3, PMMA/Al2O3-Ag, PMMA/ZrO2, PMMA/ZrO2-Ag, PMMA-Ag) nanocomposites for low cost electronics and optics applications," Transactions on Electrical and Electronic Materials, vol. 21, no. 1, pp. 48-67, 2020, [Online]. Available: https://doi.org/10.1007/s42341-020-00000-0.

[31] R. Kaliyaperumal, K. Nagaraj, and V. K. Poovan, K. Sakthikumar, C. Govindasamy, and A. S. Sivakumar, "Hydrothermal implementation with Zirconia: synthesis, characterization and investigation of biocidal activity of Ag/ZrO2 nanocomposites," Zeitschrift für Physikalische Chemie, vol. 238, no. 2, pp. 209-221, 2024, [Online]. Available: https://doi.org/10.1515/zpch-2024-0000.

[32] X. Wang, H. Cheng, Y. Min, X. Li, L. You, and J. Li, "Fe3O4@m-ZrO2@Ag ternary magnetic nanocomposites for sensitive SERS sensing and photocatalytic removal of Cr(VI) and organic dyes," Composites Part B: Engineering, vol. 239, 109959, 2022, [Online]. Available: https://doi.org/10.1016/j.compositesb.2022.109959.

[33] N. N. Jandow, N. F. Habubi, S. S. Chiad, I. A. Al-Baidhany, and M. A. Qaeed, "Annealing effects on band tail width, Urbach energy and optical parameters of Fe2O3:Ni thin films prepared by chemical spray pyrolysis technique," International Journal of Nanoelectronics and Materials, vol. 12, no. 1, pp. 1-10, 2019.

[34] H. T. Salloom, E. H. Hadi, N. F. Habubi, S. S. Chiad, M. Jadan, and J. S. Addasi, "Characterization of silver content upon properties of nanostructured nickel oxide thin films," Digest Journal of Nanomaterials and Biostructures, vol. 15, no. 4, pp. 1189-1195, 2020.

[35] S. S. Chiad, H. A. Noor, O. M. Abdulmunem, N. F. Habubi, M. Jadan, and J. S. Addasi, "Optical and structural performance of nanostructured Te thin films by (CSP) with various thicknesses," Journal of Ovonic Research, vol. 16, no. 1, pp. 35-40, 2020.

[36] C. Wang, B. Song, and Z. Zeng, "Excellent selector performance in engineered Ag/ZrO2:Ag/Pt structure for high-density bipolar RRAM applications," AIP Advances, vol. 7, no. 12, 2017.

[37] T. V. Nguyen, V. Do Truc, L. P. Thi, T. A. Nguyen, and D. L. Tran, "Self-cleaning and antibacterial polyurethane coatings with ZrO2-Ag hybrid nanoparticles," Colloid and Polymer Science, vol. 302, no. 2, pp. 225-236, 2024.

[38] M. O. Dawood, S. S. Chiad, A. J. Ghazai, N. F. Habubi, and O. M. Abdulmunem, "Effect of Li doping on structure and optical properties of NiO nano thin-films by SPT," in AIP Conference Proceedings, vol. 2213, p. 020102, 2020.

[39] E. H. Hadi, D. A. Sabur, S. S. Chiad, N. F. Habubi, and K. H. Abass, "Physical properties of nanostructured Li-doped ZrO2 thin films," Journal of Green Engineering, vol. 10, no. 10, pp. 8390-8400, 2020.

[40] H. Alfannakh and B. Souayeh, "Computational assessment of ZrO2-Al2O3/EG and ZrO2-Al2O3-Cu/EG nanomaterial on Blasius-Rayleigh-stokes flow influenced by an aligned magnetic field," Processes, vol. 11, no. 10, p. 2860, 2023.

[41] A. Kasikov and L. Aarik, "Calculating the Absorption Edge of Thin Films," Bulgarian Journal of Physics, vol. 51, no. 4, 2024.

[42] M. Alrahili, "Beyond extinction efficiencies to molar extinction coefficient of silver nanoparticles," Russian Journal of Physical Chemistry B, vol. 18, no. 1, pp. 343-356, 2024.

[43] P. Karakasis, D. Patoulias, N. Fragakis, and C. S. Mantzoros, "Effect of glucagon-like peptide-1 receptor agonists and co-agonists on body composition: Systematic review and network meta-analysis," Metabolism, vol. 164, 156113, 2025.

[44] J. Das and J. M. Kalita, "Synthesis and Development of ZrO2 Film-Based X-ray Sensor for Nondestructive Testing and Medical Imaging Applications," ACS Applied Electronic Materials, vol. 7, no. 11, pp. 4946-4960, 2025, [Online]. Available: https://doi.org/10.1021/acsaelm.5c00000.

[45] M. Chelly, D. Morganti, G. M. Abdullah, A. Tariq, G. Neri, E. Fazio, and C. Corsaro, "Optimization of ZrO2-based electrode materials for simultaneous electrochemical sensing of dopamine, uric acid and tyrosine," Materials Today Communications, vol. 45, 112254, 2025, [Online]. Available: https://doi.org/10.1016/j.mtcomm.2025.112254.

[46] J. Qian, H. Fan, S. Wang, W. Zhou, Y. Ren, C. Chen, and J. Fu, "Inverse ZrO2/Co Catalyst Enables Robust and Efficient Glucose Hydrogenation," Green Chemistry, 2026, [Online]. Available: https://doi.org/10.1039/D6GC00000A.

[47] A. S. Mokrushin, E. P. Simonenko, N. P. Simonenko, K. A. Bukunov, P. Y. Gorobtsov, V. G. Sevastyanov, and N. T. Kuznetsov, "Gas-sensing properties of nanostructured TiO_2-xZrO_2 thin films obtained by the sol-gel method," Journal of Sol-Gel Science and Technology, vol. 92, no. 2, pp. 415-426, 2019, [Online]. Available: https://doi.org/10.1007/s10971-019-04996-0.

[48] V. R. Kumar, K. K. Kumar, L. Vijayalakshmi, J. Lim, and N. Veeariah, "Optimized reddish-orange emission in Pr3+ ions doped Pb3O4-ZrO2-B2O3-SiO2 glasses for advanced photonic applications," Journal of Non-Crystalline Solids, vol. 673, 123878, 2026, [Online]. Available: https://doi.org/10.1016/j.jnoncrysol.2025.123878.

[49] A. Alruwaili, M. O. Alziyadi, M. J. Alawi, and M. S. Shalaby, “Tuning structural, dielectric constants, optoelectrical parameters, and linear/nonlinear optical features of PVC/ZrO2 nanocomposite films for flexible electronic devices,” Journal of Inorganic and Organometallic Polymers and Materials, vol. 35, no. 5, pp. 3786-3801, 2025, [Online]. Available: https://doi.org/10.1007/s10904-025-00000-0.

[50] R. Vidrio, Y. Tong, J. Liu, B. Schneider, W. O. Nachlas, N. Curtis, and J. T. Choy, “Mapping optical, chemical, structural features in ZrO2 via cross-sectional SEM-Cathodoluminescence correlation microscopy,” arXiv preprint arXiv:2601.19428, 2026.

[51] V. Subramaniyam, N. Eswaramoorthy, and J. Balasundaram, “Current status and outlook of Zr, ZrO2, and ZrS2 quantum dots: a review,” Chemical Papers, pp. 1-28, 2026, [Online]. Available: https://doi.org/10.1007/s11696-026-00000-0.

[52] H. Baqiah, M. M. A. Kechik, J. Pasupuleti, N. Zhang, N. M. Al-Hada, C. F. Chau, and S. Xu, “Nanostructure, optical, electronic, photoluminescence and magnetic properties of Co-doped ZrO2 sol-gel films,” Results in Physics, vol. 55, 107194, 2023, [Online]. Available: https://doi.org/10.1016/j.rinp.2023.107194.

[53] S. Kavitha and M. Kurian, “Effect of zirconium doping in the microstructure, magnetic and dielectric properties of cobalt ferrite nanoparticles,” Journal of Alloys and Compounds, vol. 799, 147-159, 2019, [Online]. Available: https://doi.org/10.1016/j.jallcom.2019.147159.